Journal of Multidisciplinary Engineering Science Studies (JMESS)
ISSN: 2458-925X
Vol. 6 Issue 1, January - 2020

Determination Of Subsurface Coastal Dispersions Using Dye Plum Contour Simulation And Spatial Segmentation Analysis

Okuroghoboye D. Itugha
Department of Civil & Electrical/Electronic Engineering,
Federal University Otuoke, Bayelsa State, Nigeria.
Email: diepitu@yahoo.com

Emmanuel E. Jumbo
Department of Mechanical Engineering,
Niger Delta University, Bayelsa State, Nigeria,
Email: dredjumbo@yahoo.com

Efosa Obaseki
Department of Mechanical Engineering,
Federal Polytechnic, Nekede, Imo State, Nigeria,
Email: efoba@yahoo.com

Abstract- Solute injection into natural sediments was carried out during the low ebb-water (soil was unsaturated) at the subsurface foreshores of River Mersey Estuary (RME) and monitored from 2 tidal cycles (Day-1) to Day-5. The average size of the recovered plumes' images (width) = $\bar{x}'$, and vertical length = $\bar{y}'$ relative to the depth of injection below the surface of the beach-sand were determined from the measured data. Spatial segmentation and calibration of the plumes for mean diameter, radius-ratio, etc. were also measured using Image Pro Plus (IPP) caliper submenu along the major and minor axes for the vertical and width cross-sectional lengths respectively. The concentration information was estimated out of the photographic images of the plumes. A Gaussian model in MATLAB was applied on the calibrated plume data to simulate the contours of concentration curves described in the data points. It enabled the interpretation of the patterns of observed plume images recovered from the field so that we have results of the dispersive parameters associated to the distribution of the chemical. The results show that coefficient of apparent dispersion was not constant as shown in the longitudinal concentration curves. The non-uniformity may be associated to the varying phenomenon of mechanical processes affecting flow in the subsurface as indicated in the concentration curves/plumes which can be attributed to a combination of environmental consequences.

Keywords—Coastal foreshore, dye tracer, dispersion, plume images, interstitial hydraulics.

I INTRODUCTION

Though the movement and transport of dissolved pollutants in the subsurface have intensively been researched for several decades both with analytical and numerical theories [1] [2], the studies have been mainly on groundwater and less in beach-sand (vadose zone). A review on groundwater behavior in sandy beaches with the relationship between tides and beach water-tables can be found in [3] [4]. The main drivers of dispersion are attributable to the interplay of intermolecular cohesive forces referred to as convection and molecular diffusion [5]. For instance, the movement of the plume affected by spread is assumed to be the role of hydrodynamic dispersion in the complexly structured vadose zone. This according to [6]. Further views discussed in [7] arose from impressed pressure affecting the velocity field in the media which have craved the attention of many authors into expressing the hydrodynamic dispersion coefficients as a function of the Peclet number [8], [9], [6], [10], [11]. The authors have applied several techniques including acoustic, radioactive tracers, etc., to investigate changes in solute concentration. Also, literature on the use of analytical solutions to the problem of unsaturated-saturated flow in coastal environments for the description of concentration distribution in the subsurface exists.

One relatively recent study that coupled the unsaturated and saturated zone is the work of [12] who presented transient and steady state analytical solutions to predict sub-surface migration of a surface released contaminant. The main issue in applying the advection-dispersion equation (ADE) analytical solutions is the restriction that equation parameters will have to be treated as constants [12]. This implies that the variation of water/injectate (dye solute) movement in the vadose zone due to tidal and groundwater exchanges through time will be approximated by constants. The approximation results

from observations that the distance and time intervals are often and usually very small compared to tracer/water movement and transport in groundwater aquifers and river channels [13], [14].

Further, [15] and [16] reflected that the varieties of ways oscillatory tides interact with groundwater flow fields do influence the dynamic regime of hydrology in subsurface coastal foreshores. The importance attached to studies of this nature lie in the understanding that controlled waste storage and disposal activities in coastal vadose zones can have significant effects on the habitat. This is because the vadose zone has direct link to groundwater aquifers and the surface-water, so all three phases may become vulnerable to contamination in the event of major pollution affecting one. In particular, controlled urban/industrial waste storage and disposal in the vadose zone can affect surface and groundwater as found in this study. It has also shown that salinity can induce pore water to transport dissolved solutes by convection due to density sensitivity [17]. In the present study, salinity levels recorded in the saturated depths of the beach sand were on average found to be slightly higher (1.28%) compared to the surface seawater, which describes accumulated trends of salinity infiltration.

The assumption here is that oscillatory tides offset the undersurface dye solute during the unsaturation-saturation phases of flow by impressing greater velocities at the surface of the foreshores. This results into causing processes affecting the movement and transport (such as diffusive mixing, advective dispersion, etc.) of the plumes across the porous medium. To clarify understanding of the processes (movement and transport) involved, the ADE was used to try analyzing and interpreting the movement and fate of the injectate (dye solution) in the vadose zone. The concentration information was estimated out of the photographic images of the plumes.

Coastal studies of this nature are essential especially to environmental engineering science, hydro-geological and aquifer management studies because they enable provide understanding through quantifying and prediction of chemical (nutrients or contaminants) migration pathways. Early detection of such events can enable on-time preparations and decisions to be made especially on alternative remedial approaches and help minimize risks to habitats.

IIDESCRIPTION OF STUDY AREA, EXPERIMENTAL DESIGN, METHOD AND DIGITAL-IMAGE PROCESSING

A. Study site

All five (5) experimental sites [18] are located at the coastal foreshores of the Liverpool Bay (outer estuary injection site (OEIS) with 3 injection zones (IZ)) and Narrows (narrows estuary injection site (NEIS) with 2 injection zones (IZ)) of the RME, NW England (53°26′N and 003°02′W). At the OEIS we have IZ (A, B, and C) and at the NEIS are IZ (A and B). The historic and socio-economic significance of the catchment, such as urban/industrial waste and sewage sludge discharge information, can be found in literatures [19], [20], [21]. The water levels at the experimental sites are nearly the same as in the sea. During low tides, large portions of the intertidal foreshore are exposed. The median grain size (d_{50}) of the exposed foreshore varies spatially with the range from 0.196mm to 0.259mm. The strong tides can reach about ± 5m while the mean tides vary at less than ±2m.

B. Experimental design, tracer applied and method

Solute injection into the natural sediments was carried out during the low ebb-water (soil was unsaturated) and monitored from 2 tidal cycles (Day-1) to Day-7. The positions of injection points (IPs) were marked using a 12-channel Garmin GPS 76 marine navigator. At the expiration of each monitoring phase the respective locations of the IPs were identified and excavated carefully to penetrate the undisturbed plume domain. The design was such that each sampling point (SP) contains 3 x 5 IPs over 0.5m x 0.5m square cells in 1.5m x 2.5m rectangular arrays. Out of over 590 x 3 IPs initiated at the five (5) sites, a total of about 322 x 3 samples were successfully obtained, filmed/photographed (using Nikon Coolpix 8800 digital camera with 8.0 effective megapixels) and measured in the field.

The injectate is a Red Colour 810 permitted food solvent, colour (E124) with 4.3% pure dye content. A 5ml (0.215g) was injected using a 10ml syringe perpendicularly into the unsaturated natural beach-foreshore. The plumes that penetrated the water table region (12^{th} to 14^{th} tidal cycles) were not considered since the plume-fronts could not be accessed.

Fig 1: Spatial segmentation and calibration of observed plumes for mean plume parameters

III QUANTIFICATION OF PLUME IMAGES

To quantify the geometric profiles of the image plumes obtained from the field, preliminary tests were conducted in the laboratory with dried samples of the field sediments. The method involves construction of rectangular boxes with volumetric dimension 9.2x7.8x2.0cm^3. The depth of field materials (completely dry sand) introduced was approximately 1.2cm, such that the volume of sand introduced into the box (es) on each test occasion was 9.2x7.8x1.2cm^3. Initially 10ml of undiluted injectate (dye) solute was introduced and allowed to be absorbed, and then photographed perpendicularly above the cross-section of the box. The solute sample with concentration 43mg/L was then diluted using calculated amounts of water (0.001 to 0.0099L) to vary from 0 to 0.043mg/L. The Nikon camera recorded the images in jpg format which were converted to the lossless tiff file type for the image analysis.

The intensity of the black and incident or background levels was first established as 1 and 115 respectively, which were entered in the optical density calibration box. The density-distance plots were obtained through the line profile command after several protocol options provided by the IPP including the statistical submenu. The statistical data was exported to Microsoft Excel for further processing while the plots were saved into image tiff files using the IPP screen capture utility (Fig. 1). A relative concentration profile, $C_r = \mathrm{m}\rho_{opt}{}^{a}$ could be represented from a least square fit when the intensity data was standardized to optical density. The value '*a*' refers to indicial power showing nonlinearity in the relation. The concentration data of the injectate images here was obtained using the nonlinear indicial power relation, $C = 0.3509 * \rho_{opt}{}^{5.3238}$.

A. Digital-image processing model

The spatial data was quantified by using computer imaging techniques to convert the two-dimensional (2D) photo-images to digital formats with a 1/300th pixels per inch resolution [22], [23]. Concentration information was obtained from the tests conducted in the laboratory with dried samples of the beach-sand and related to the optical density intensity of the plume [24].

The mean diameters, radius-ratios and areas of the plume were analyzed using the image processing tools, image-pro plus (IPP) and Matlab. The radius-ratio is a measure derived from taking the maximum radius of the plume divided by its minimum radius. The average size of the plumes (width) = $\bar{x}'$, and vertical length = $\bar{y}'$ relative to the depth of injection below the surface of the beach-sand were determined from the measured data. The mean diameter of the plume, and radius-ratios, etc. were also measured using the IPP caliper submenu along the major and minor axes for the vertical and width cross-sectional lengths respectively (Fig. 1). The average length of diameters was measured at 2 degrees intervals through the plumes' centroids. The radius-ratio was measured using the ratio between the maximum radius of the plume and its minimum radius. Measurements were taken from the sand-surface through in the direction of the water table.

The concentration data were then obtained using the nonlinear indicial power relation $C = 0.3509 * \rho_{opt}{}^{5.3238}$ from the laboratory calibrations, where C is dye concentration; ρ_{opt} is the optical density intensity, $\left[\rho_{opt} = \log_{10}(m/I)\right]$, where *m* is a constant, and I (= (Red + Green + Blue)/3) is the light intensity (*see* Zhang et. al 2002 and Huang et. al 2002 for more details).

Individual calibration of the transverse and longitudinal dispersion of the plumes was done, where the Gaussian Operator in Matlab $C(x) = ae^{\left[-((x-b)/\sigma)^2\right]}$ describing the concentration was applied such that, σ = peak width of plume distribution or mixing length/width, b = peak location of center of plume and $a = \left(\sqrt{4\pi Dt}\right)^{-1}$ = peak amplitude and $D = \sigma^2/4t$ = apparent dispersion; and the slope method $D_x = \left(4m_x t\right)^{-1}$, and $D_y = \left(4m_y t\right)^{-1}$ where m_x = transverse slope, m_y = longitudinal slope. SSE = sum of squared errors, RMSE = root mean square error (Table 1).

B. Results and Analysis

Variations in transport in laboratory experiments

Figs (2-3) represent the output from the laboratory data with the 50/50% water-chemical ratio using the bi-harmonic operator in MATLAB. It describes the behaviour of the concentration in the longitudinal cross-section of the dry sand. The variations in the data points demonstrate that the measurement errors do not have equal variance. It implies that their variance is proportional to the maximum peak of the mean curve. The Gaussian trend in the bi-harmonic surface therefore analyzes the data into a model by predicting the response variable. The mean response described by the Gaussian behaviour minimizes the measurement errors between the best-fit curve and experimental data which shows the peak concentration path as symmetric. That is, the fit-result (x,y) refers to the bi-harmonic surface where x, y are normalized by means 0.0267 and 0.0103 with standard deviations 0.01543 and 0.001543 respectively. Fig (3) describes the concentration path spatially by means of a contour which peaked between the points (2.7, 1.43) cm and (3.5, 1.48) cm.

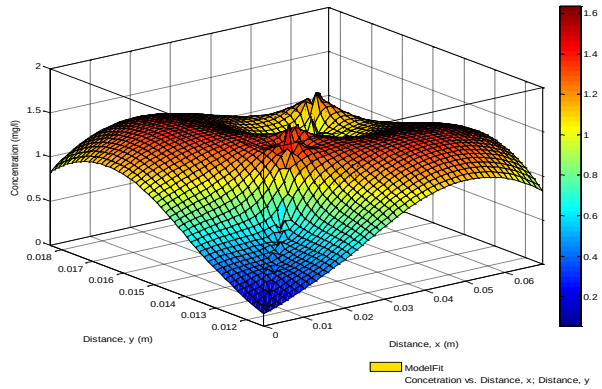

Fig 2: Spatial description of the concentration (longitudinal) in the laboratory using bi-harmonic interpolation along x and y. The color-bars show the variation of concentration in the longitudinal plane.

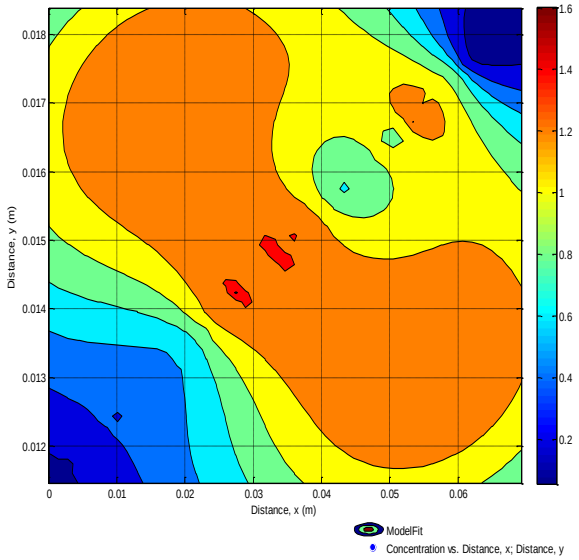

Fig 3: Spatial description of the concentration (longitudinal) in the laboratory using contours along x and y. The color-bars show the variation of concentration parallel to the solute flow direction.

IV DETERMINATION OF LONGITUDINAL DISPERSION COEFFICIENT

A. Variations in the longitudinal transport from Day-1 to Day-5

The vertical concentration curve derived from the longitudinal cross-section of the plumes at the OEIS-IZ (A) sampling points for Day-1 is shown in Fig (4). The curve is asymmetrically skewed to the left, which is uniquely non-Gaussian and may imply that the sand in the vertical path has relatively non-isotropic packing. The individually calibrated plume also reveals higher concentration contrast in the longitudinal flow path. The observed concentration path is characterized by several non-periodic peaks due to non-uniform solute movement, showing the effect of advective diffusion mechanism. The calibrated D_{hL} [$D = \sigma^2/(4t)$] value using the Matlab model 'Gaussian' operator is $5.208x10^{-05}m^2/hr$ by the slope method for the whole 65 plumes for Day-1. These values compared to the estimate $2.839x10^{-04}m^2/hr$ for the entire OEIS-IZ (A) site comprising data from Day-1 to Day-5 are about 3 to 6 times lower respectively. The assumed constant velocity 0.003475m/hr is derived from the first order moments curve for the OEIS-IZ (A) zone. The goodness-of-fit estimates are in (Table 1) showing that the model fits the observed data well.

The 3D Gaussian bi-harmonic interpolation (Fig 5) of the case in Fig (4) is computed from the coefficient structure where x and y are normalized by the means 0.0152 and 0.0355 with the standard deviation 0.002 and 0.021 respectively. The variation of concentration (color bar) is described in the bi-harmonic surface as asymmetric non-Gaussian profile. The asymmetric behaviour of the concentration distribution can also be demonstrated in terms of contours (Fig 6). The contours, just as in the 2D and 3D surface plots, show the concentration front of the plume to be increasing as it converges/narrows vertically further into the depth of the sediments up to the point (1.75, 6.00) cm.

Also, the longitudinal cross-section of the lone plumes for Day-2 is represented in Fig (7). The data points reveal multiple peaks in the observed distribution associated to the trend of concentration, which may relate to the complexity in the movement and transport. The effect of the Gaussian operator shows in solid line the path describing concentration distribution which considerably minimized the errors (Table 1). The Gaussian profile of the concentration values is asymmetrically left-skewed. The asymmetry uniquely shows that the concentration profile is non-Gaussian, hence, the sand in the vertical profile may relate to a fairly non-isotropic packing. This also may relate to the several non-periodic peaks and the non-uniform solute movement, showing the effect of advective diffusion mechanism. The estimated individually calibrated apparent dispersion value, $6.8x10^{-05}$ m^2/hr from the Gaussian model and $2.167x10^{-04}$ m^2/hr from the slope method for the entire Day-2 data, all increased with distance compared to the previous case. However, the effective dispersion coefficient for this site [OEIS-IZ (A)] estimates to $2.839x10^{-04}m^2/hr$ using the slope method which comprises Day-1 to Day-5. The behaviour described in the visual shapes of the plumes may therefore be associated to inhomogeneity in the beach-sand as the injectate advances into the less conductive regions [25].

The observed concentration curves in Fig (8) representing plume behavior of Day-3 at the OEIS-IZ (A) shows negatively skewed Gaussian distribution. The Gaussian simulation of the longitudinal effective dispersion coefficient for this plume is $7.077x10^{-05}m^2/hr$ against the value for the entire Day-3 data $3.600x10^{-04}m^2/hr$ using the slope method. The model described the observed data well as shown in the small RMSE value of 0.024 with R-squared of 95.1%. The behaviour of the plume's longitudinal cross-

section corresponds to earlier patterns already discussed, showing the spread in the concentration.

The plume as represented in the concentration curve in Fig (9) belongs to Day-4 travel time data averaging about 98.83±0.49hrs. The Gaussian model fitted the observed data well showing left-skewed longitudinal concentration peaks which corresponds to observations described above. The shapes of the plumes described in the curves may be attributable to ambient velocity dispersion trends but hydraulic conductivity observed in the vicinity was not applied, hence no discussion on its influence. The asymmetry described by the distribution may relate to constraints in the vertical plane due to relative inhomogeneity or near-water table region factors in the subsurface. The individually calibrated effective longitudinal dispersion coefficient from the Gaussian model for this plume is 5.318E-05m^2/hr and the estimated value using the slope technique is1.377E-04m^2/hr for the entire Day-4 data of the OEIS-IZ (A) zone.

The asymmetric profile of the longitudinal cross-section of the plumes at the OEIS-IZ (A) for Day-5 is presented in Fig (10). The asymmetry in the distribution suggests the profile is far from symmetry hence the composition of the sediment material may be relatively different. The longitudinal dispersion coefficient due to the Gaussian model is 9.375x$10^{-05}$$m^2$/hr compared to the slope technique value of 3.486x$10^{-04}$$m^2$/hr for the entire Day-5 data for the OEIS-IZ (A) region. The later value representing this particular plume is about 3 times less while the latter is equivalent, all in comparison to the effective hydrodynamic longitudinal dispersion coefficient for all plume data.

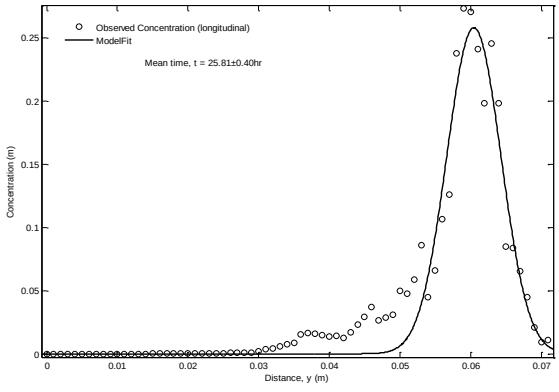

Fig 4: A Day-1 2-D Gaussian plume model showing non-Gaussian asymmetric behaviour of the transport (longitudinal) of dye concentration in the sediment as a function of distance under natural oscillatory tides. The solid line indicates the 'Gaussian' asymmetry in the behaviour of the plumes.

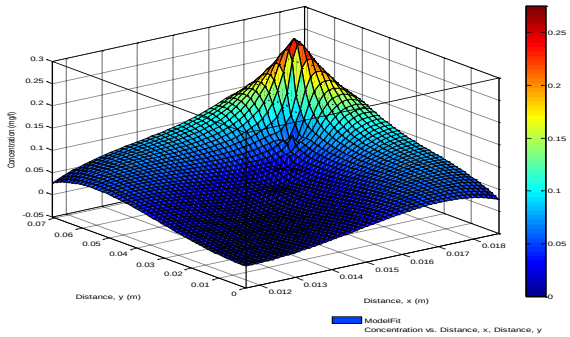

Fig 5: 3D spatial description of the concentrate (longitudinal) on (Fig 4) using bi-harmonic interpolation along x and y. The color-bars show the variation of concentration.

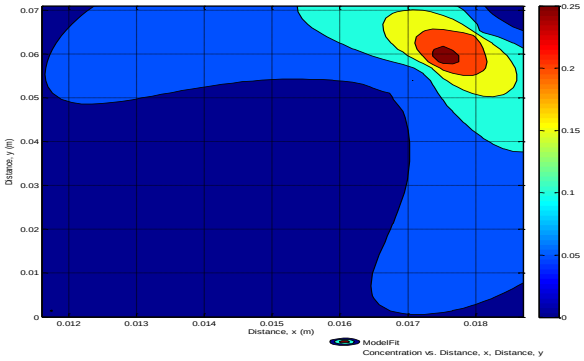

Fig 6: Spatial description of the concentration (longitudinal) in SP-1 (Fig 4) using contours along x and y. The color-bars show the variation of concentration.

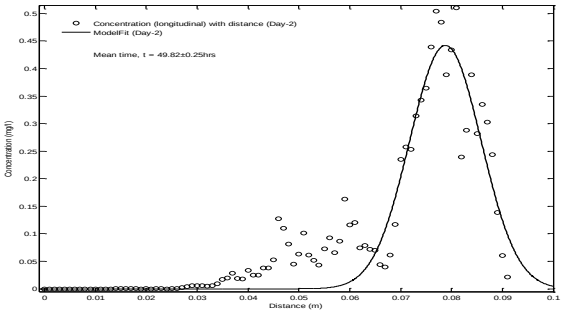

Fig 7: Day-2 2-D Gaussian model showing non-Gaussian asymmetric behaviour of the transport (longitudinal) of injectate concentration in the sediments as a function of distance under natural oscillatory tides. Solid line indicates the 'Gaussian' fit.

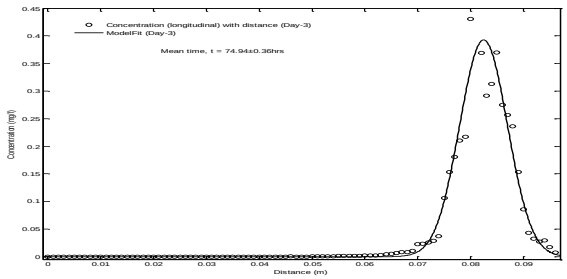

Fig 8: Day-3 2-D Gaussian model showing non-Gaussian asymmetric behaviour of the transport (longitudinal) of injectate concentration in the sediments as a function of time under oscillatory tides.

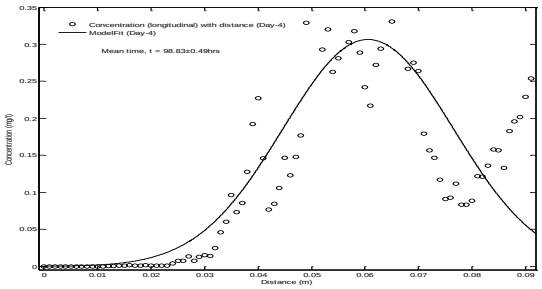

sediments with time under natural oscillatory tides.

Fig 9: Day-4 2-D Gaussian model showing non-Gaussian asymmetric behaviour of the transport (longitudinal) of solute concentration in the sediments under oscillatory tides.

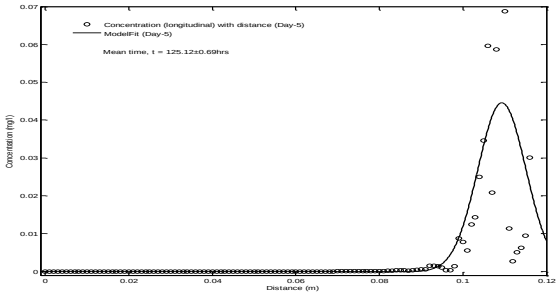

Fig 10: Day-5 2-D Gaussian model showing non-Gaussian asymmetric behaviour of the transport (longitudinal) of injectate concentration in the

Table 1: Longitudinal [D_{hL} (m^2/hr)] dispersion coefficients obtained using the Gaussian operator[1], with values from the slope or simultaneous technique.

Longitudinal cross-sections of plumes						
Time (hr)	σ (m)	Gaussian D_{hL} (m^2/hr)	Slope D_{hL} (m^2/hr)	SSE	R-square	RMSE
25.81±0.40	0.005428	5.208E-05	9.253E-05	0.0257	0.9291	0.0193
49.82±0.25	0.009957	6.800E-05	2.167E-04	0.2396	0.8636	0.05188
74.94±0.36	0.006405	7.077E-05	3.600E-04	0.05327	0.9507	0.02381
98.83±0.49	0.02256	5.318E-05	1.377E-04	0.3798	0.7391	0.06533
125.12±0.69	0.008147	9.375E-05	3.486E-04	0.01712	0.4948	0.0122

V. SUMMARY AND CONCLUSION

The IPP in addition to MATLAB scripts have been successfully applied to process 2-D colour images of dye plumes recovered in the RME subsurface foreshores, as required in non-invasive techniques (Robbins 1989). Thus conventional techniques are incorporated to enhance clarity in this unique problem of solute movement and transport in coastal sediments which is different to solute transport in GW aquifers.

A Gaussian model in MATLAB was applied on calibrated plume data to simulate the contours of concentration curves described in the data points. It enabled the interpretation of the patterns of observed plume images recovered from the field so that we have results of the dispersive parameters associated to the distribution of the chemical. The effective dispersion coefficient estimates determined simultaneously [26], using slopes derived from the ADE were compared to the individually calibrated results using the Gaussian operator in Matlab. Descriptions of these data for all experimentation zones with 95% confidence intervals are shown in Table 1. The results show that coefficient of apparent dispersion was not constant as shown in the figures of longitudinal concentration curves. The analyses show that the non-uniformity may be associated to the varying phenomenon of mechanical processes affecting flow in the subsurface as indicated in the concentration curves/plumes. The erratic patterns observed in the concentration curves were relatively particular to early times in the experiments after solute injection especially in the longitudinal flow of winter season. Also, the patterns of plume response may not be attributable to singular but combinations of environmental consequences. The uniqueness of the findings may therefore need further investigations or clarifications particularly the influence due to

permeability, the semi-diurnal tides and the role of salinity using numerical methods.

However, it is reasonable to suggest that the SW and GW connected to the vadose zone of the study field are vulnerable to diffuse contaminants.

The individually calibrated profiles of the plumes show that the surficial zones of the study area may be relatively uniform (homogeneous and isotropic) in relation to the plume structure deeper into the subsurface direction of flow. This is in agreement with the laboratory data except for the vertical directions of flow where the concentration curves deviate in the field results to describe unique patterns of asymmetry or non-Gaussian trends. The asymmetry here is associated to relative inhomogeneity and anisotropy of the beach-sand in the vertical terrain (lower depths) approaching the vicinity of the water table. It shows the characteristics associated to mediums reflecting similar properties such as decreasing hydraulic conductivity, increasing dispersion and concentration. In-spite of the 2D Gaussian models applied to data, the behaviuor of the plumes has also been described using bi-harmonic surface interpolations and contours to portray the different aspects of the movement and transport phenomenon.

The dynamic exchange phenomenon between GW and SW driven by semidiurnal tides synonymous with the study terrain is responsible in causing significant flux activity at the outer RME beach. This flux activity has the potential to drive or transport diffuse nutrients and contaminants either into the GW or SW or both simultaneously in the study field.

VII REFERENCES

[1] C. W. Fetter, (1999) Contaminant Hydrogeology. Second Edition, Prentice Hall Upper Saddle River, NJ07458.

[2] E. B. Diaw, P. Lehmann, and F. Ackerer (2001). One-dimensional simulation of solute transfer in saturated–unsaturated porous media using the discontinuous finite elements method. Journal of Contaminant Hydrology, Volume 51, Issues 3-4, October, Pages 197-213.

[3] A.J. Baird and D.P. Horn. (1996) Monitoring and modeling groundwater behaviour in sandy beaches. Journal of Coastal Research **12**(3): 630–640.

[4] B. Berkowitz, I. Dror and B. Yaron, (2008). Contaminant Geochemistry: Interactions and Transport in the Subsurface Environment. Springer-Verlag Berlin Heidelberg.

[5] R. Aris, (1956), On the dispersion of a solute in a fluid flowing through a tube. Proc. R. Soc. Lond. A 1956 Volume 235, Pages 67-77; DOI: 10.1098/rspa.1956.0065. Published 10 April 1956.

[6] M. Sahimi, (1995). Flow and Transport in Porous Media and Fractured Rock: From Classical Methods to Modern Approaches, VCH, Weinheim.

[7] M. Sahimi, B.D. Hughes, L.E. Scriven, H.T. Davis (1986), Dispersion in flow through porous media—I. One-phase flow. Chem. Engng Sci. 41, 2103–2122.

[8] G. Drazer, R. Chertcoff, L. Bruno, M. Rosen, and J. P. Hulin (1999). Tracer dispersion in packings of porous activated carbon grains. Chem. Eng. Sci. 54, Pages 4137-4144.

[9] G. Drazer, and J. Koplik, 2001. Tracer dispersion in two-dimensional rough fractures. Phys. Rev. E 63, 056104/1-11.

[10] E.J. Peters, R. Gharbi, and N. Afzal (1996), A look at dispersion in porous media through computed tomography imaging. J. Petr. Sci. Engng 15, 23–31.

[11] B. Manz, P. Alexander, L.F. Gladen, (1999), Correlations between dispersion and structure in porous media probed by nuclear magnetic resonance. Phys. Fluids 11, 259–267.

[12] L.D. Connell, (2007). Simple models for subsurface solute transport that combine unsaturated and saturated zone pathways. Journal of Hydrology 332, pp361– 373

[13] W. Czernuszenko, and P. M. Rowinsky (1997), Properties of the dead-zone model of longitudinal dispersion in rivers. J. of Hydraulic Research, 35 (4), 491-504.

[14] M.J. Lees, L.A. Camacho and S.C. Chapra, (2000), On the relationship of transient storage and aggregated dead-zone models of longitudinal solute transport in streams. Water Resources Research 36(1): 213–224.

[15] M.C. Boufadel, (2000). A mechanistic study of nonlinear solute transport in a groundwater–surface water system under steady state and transient hydraulic conditions. Water Resources Research, Vol. 36, No. 9, 2549–2565, September 2000.

[16] L. Li, D.A. Barry, F. Stagnitti, J.Y. Parlange, D.S. Jeng, (2000), Beach water table fluctuations due to spring-neap tides: moving boundary effects. Advances in Water Resources 23 pp817-824

[17] C. Rocha, (2000), Density-driven convection during flooding of warm, permeable intertidal sediments: the ecological importance of the convective turnover pump. Journal of Sea Research 43, pp1-27.

[18] D. O. Itugha, D. Chen, and Y. Guo (2016), Pollutant advective spreading in beach sand exposed to high-energy tides. Estuarine, Coastal and Shelf Science, Vol.181, pp.70-82, http://dx.doi.org/10.1016/j.ecss. 2016. 08.011. 2016 Elsevier Ltd.

[19] P. D. Jones, (2006). Water quality and fisheries in the Mersey estuary, England: A historical perspective. Marine Pollution Bulletin 53, pp144–154.

[20] A.J. King, J.W. Readman and J.L. Zhou (2004), Determination of polycyclic aromatic hydrocarbons in water by solid-phase microextraction - gas chromatography - mass spectrometry. Analytica Chimica Acta B, 523(2): 259-267.

[21] H. R. Rogers, (2002), Assessment of PAH contamination in estuarine sediments using the equilibrium partitioning–toxic unit approach. Sci Total Environ. 290:139–55.

[22] B.A. Harrison, (1990). Introduction to Image Processing, CSIRO Australia, 256p.

[23] J.C. Russ, (1992). The image processing handbook. CRC Press Inc, 445 p.

[24] R.A. Schincariol, E.E. Herderick, F.W. Schwartz. (1993). On the application of image analysis to determine concentration distributions in lab expts. J. Contam. Hydrol. 12: 197-215.

[25] E. Park and H. Zhan (2001), Analytical solutions of contaminant transport from finite one-, two-, and three-dimensional sources in a finite thickness aquifer. Journal of Contaminant Hydrology, 53: 41-61.

[26] J. S. Chen, C. S. Chen, H. S. Gau and C.W. Liu (1999). A two-well method to evaluate transverse dispersivity for tracer tests in a radially convergent flow field. J. Hydrology; 223(3-4): 175-97.